Wing kinematic and aerodynamic compensations for unilateral wing damage in a small phorid fly

Yu Zhu Lyu [*], Hao Jie Zhu, and Mao Sun

Ministry-of-Education Key Laboratory of Fluid Mechanics, Institute of Fluid Mechanics, Beihang University, Beijing 100191, China

To investigate the way in which very small insects compensate for unilateral wing damage, we measured the wing kinematics of a very small insect, a phorid fly (*Megaselia scalaris*), with 16.7% wing area loss in the outer part of the left wing and a normal counterpart, and we computed the aerodynamic forces and power expenditures of the phorid flies. Our major findings are the following. The phorid fly compensates for unilateral wing damage by increasing the stroke amplitude and the deviation angle of the damaged wing (the large deviation angle gives the wing a deep U-shaped wing path), unlike the medium and large insects studied previously, which compensate for the unilateral wing damage mainly by increasing the stroke amplitude of the damaged wing. The increased stroke amplitude and the deep U-shaped wing path give the damaged wing a larger wing velocity during its flapping motion and a rapid downward acceleration in the beginning of the upstroke, which enable the damaged wing to generate the required vertical force for weight support. However, the larger wing velocity of the damaged wing also generates larger horizontal and side forces, increasing the resultant aerodynamic force of the damaged wing. Due to the larger aerodynamic force and the smaller wing area, the wing loading of the damaged wing is 25% larger than that of the wings of the normal phorid fly; this may greatly shorten the life of the damaged wing. Furthermore, because the damaged wing has much larger angular velocity and produces larger aerodynamic moment compared with the intact wing of the damaged phorid fly, the aerodynamic power consumed by the damaged wing is 38% larger than that by the intact wing, i.e., the energy distribution between the damaged and intact wings is highly asymmetrical; this may greatly increase the muscle wastage of the damaged side.

I. INTRODUCTION

Insects are the smallest fliers in the world and have excellent flight performance. They can adjust the wing kinematics to achieve hovering, forward flight, climbing flight, and amazing maneuvering, even with damaged wings [1–9]. The wings of insects are prone to damage because of attacks, predation, and collisions with the environment [1]. Different from birds or bats [10,11], insects cannot renew damaged wings, hence they must compensate for the damaged wings by adjusting the wing kinematics during flight.

Loss of wing area is the most direct problem that wing-damaged insects face. In the case of identical damage of both wings, the compensation in flight is often associated with increased wingbeat frequency, flapping amplitude, and angle of attack of both wings [1–4], which is similar to the adjustment in the vertically ascending flight of normal insects [12]. For asymmetrical damage, which may be more common in the wild, insects should produce enough vertical force to support their weight while minimizing the torque produced from asymmetrical forces to maintain a balanced flight [5–8]. The kinematic compensation for this situation is more complicated, and both intact and damaged wings need to be adjusted [6].

The compensational strategies for asymmetrical wing damage are varied among different species of insects. Hawkmoths [5] compensate for unilateral wing damage through a remarkable increase in stroke amplitude on the damaged wing and an increase in the overall wingbeat frequency. Fruit flies [6] with unilateral damage adjust not only the stroke amplitude and wingbeat frequency, but also the timing of stroke reversal and the rolling angle of the body. A study about damselflies [7] indicates that even if one of the hindwings is removed, the insects can also fly and maneuver by adjusting the wingbeat frequency, flapping amplitudes, angle of attacks, and stroke plane angles of the remaining three wings.

Previous studies on kinematic and aerodynamic compensations for wing damage were performed on medium and large insects (wing length $R \approx 5-50$ mm). Recent studies have shown that the flapping mode and force production mechanism of very small insects ($R \approx 0.5-4$ mm) are very different from those of their larger counterparts [13,14]: Medium and large insects in normal hovering flight stroke the wings back and forth in an approximately horizontal plane, referred to as upstroke and downstroke, respectively [12–14]. But for very small insects, because of the very low Reynolds number (Re) or very large viscosity effect, flapping in the same way as their larger counterparts cannot produce sufficient lift [15–17]. It has been found that for small insects, as the size or Re decreases, the upstroke wing motion becomes more downward-curved (a U-shaped upstroke), which results in a stronger vertical force [13,14]. This indicates that very small insects may have different strategies to compensate for wing damage. In addition, previous works measured the oxygen consumption rates or CO_2 production rates to estimate the energy expenditures of insects with damaged wings [2,9], but it is not yet known how the insects distribute energy to the damaged wing and the normal wing.
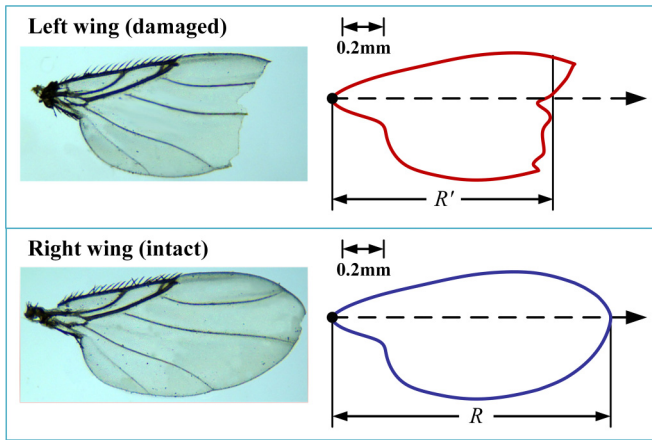
*lvyzhu@buaa.edu.cn

FIG. 1. Wing planforms of the phorid fly with a damaged left wing. R', wing length of the damaged left wing; R, wing length of the intact right wing.

FIG. 2. Sketch showing the experimental measuring apparatus.

In the present paper, we study the problem of kinematic and aerodynamic compensations for wing damage in a very small insect, namely the phorid fly *Megaselia scalaris*. Average-sized insects have a wing length around 5 mm [18], while very small insects have a wing length ranging from approximately 0.5 to 4 mm. The wing length of the phorid fly is approximately 1.3 mm, so we can consider that it is a representative very small insect. We used three high-speed cameras to measure the wing kinematics of a phorid fly with natural damage on the left wing. Based on the measured wing kinematics, we numerically solved the Navier-Stokes equations to obtain the aerodynamic forces acting on and the flows around the phorid fly. For comparison, we did the same to an intact phorid fly with almost the same morphological parameters and under the same flight conditions. We compared the flapping kinematics, aerodynamic forces, and power consumptions of these phorid flies to evaluate the kinematic and aerodynamic compensations for the unilateral wing damage, and through analyzing the flows around the wings of the wing-damaged phorid fly, the force production mechanism and energy distribution between the damaged and intact wings were also investigated.

II. MATERIALS AND METHODS

A. Wing kinematics measurement

Among the adult phorid flies (*Megaselia scalaris*) obtained from the Laboratory of Urban Integrated Pest Management and Ecological Security, Shenyang University, a small phorid fly with natural wing area loss in the outer part of the left wing was found and chosen as the subject of the current study. The planforms of the damaged wing and the intact wing of this phorid fly are shown in Fig. 1. To compare with the wing-damaged phorid fly, a normal phorid fly was selected from the same group, which has similar morphological parameters to the wing-damaged one.

We studied the steady, low-speed flights of the phorid flies using three synchronized high-speed cameras (i-SPEED 716, iX Cameras, Essex, UK) which were mounted on an optical table (Fig. 2). To satisfy the need for time and space fidelity,
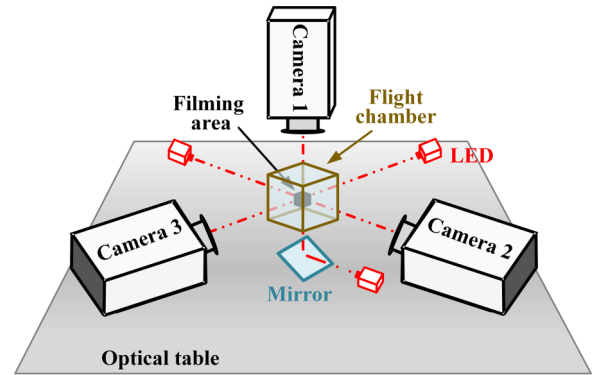
the cameras' speeds were set to 9000 frames per second (resolution 1400×1008 pixels) with the shutter speed set to 10 μs. Then each wing-beat cycle contains about 30 snapshots. Each camera was equipped with a 60 mm micro-Nikkor lens to satisfy the need for the filming area (approximately $1.5 \times 1.5 \times 1.5$ cm^3). The camera view was backlit using a 50 W integrated light emitting diode (LED; luminous flux, 4000 lm; wavelength, 632 nm). During the experiment, the phorid flies were transferred into a transparent $6 \times 6 \times 6$ cm^3 flight chamber. The synchronized cameras were manually triggered when the insect was observed to fly steadily in the filming area. The ambient temperature was kept at $25-27$ °C and relative humidity was $50-60\%$.

The insects were anaesthetized immediately after flight recording, and then the total mass of each phorid fly was measured by a laboratory balance within an accuracy of ± 0.01 mg (BT25S, Sartorius AG, Göettingen, Germany). The wing shape was captured using a microscope equipped with an electronic eyepiece (display resolution: 2048×1536). The body shape was reconstructed from the video sequences, and the body cross sections were simplified as ellipses [19].

After all the morphological parameters were obtained, we manually measured the body and wing kinematics frame by frame using a stereo-vision-based method [20,21]. The basic idea was to adjust the positions and orientations of the models of the body and wings, separately, until their projections overlapped with their counterparts on recorded snapshots in all three views. A coordinate system (X, Y, Z) with the origin at the wing root was used to describe the wing motion [Fig. 3(a)]. The X-axis points horizontally backwards, the Y-axis points vertically upwards, and the Z-axis points to the left of the insect. The inclination angle of the stroke plane about the horizontal is denoted as β. For a flat-plate wing, the stroke angle (ϕ), the pitch angle (ψ), and the deviation angle (θ) can determine the orientation of the wing [Fig. 3(a)]. A detailed description of this method can be found in our group's previous works [21,22]. Recent studies showed that very small insects appeared to have large spanwise bending on the wings [13,14]. The wing bending of this small phorid fly could also be clearly observed, thus spanwise bending was taken into account to better match the model projections and the displayed frames, as was done in Refs. [13,14] for very small insects. Based on the observations, it was assumed that maximum bending displacement (d_m) was at 40% of the wing length
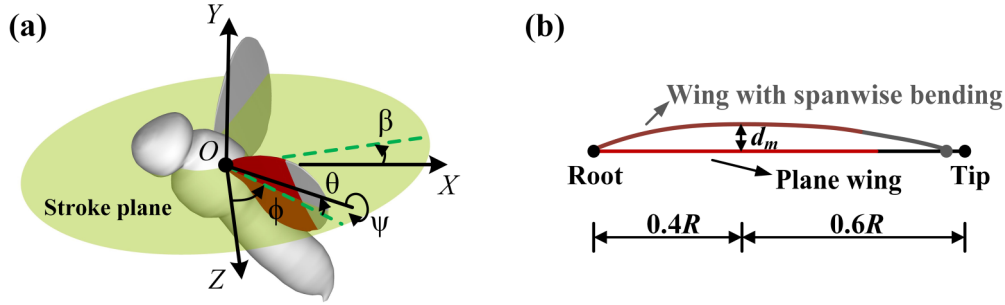
FIG. 3. Kinematic definition: (a) coordinate system (X, Y, Z) with origin at the wing root and Euler angles defining the wing kinematics; (b) definition of the spanwise bending.

from the wing root [Fig. 3(b)]. The bending distribution along the wingspan is approximated as follows: Let r represent the spanwise distance. The bending distribution between $r/R = 0$ and 0.4 is a quadratic curve, and so is that between $r/R = 0.4$ and 1 [Fig. 3(b)]. Therefore, the bending distribution is determined by one parameter, d_m, which is determined in the process of matching the model image and the displayed frame. From the picture of the wing shown in Fig. 1, it is seen that the wing veins are much thicker between $r/R = 0$ and $r/R \approx 0.4$. This is most possibly the reason why the maximum bending is at $r/R \approx 0.4$. For the damaged wing, the wing area loss is at the outer part of the wing (between $r/R \approx 0.8$ and $r/R = 1$), and the part between $r/R = 0$ and $r/R \approx 0.4$ where wing veins are thick is not affected. Therefore, the maximum bending also appears at $r/R \approx 0.4$.

In a previous paper of our group [22], an error analysis of the method of wing-kinematics measurement was performed. It was shown that the primary errors of the method were due to wing deformation (spanwise twist and chordwise camber deformations) and discretization. The wing deformation errors and discretization errors were estimated on the whole by applying the method to a computer-generated virtual hoverfly, the twist and camber deformations of which were known. It was shown that errors in the positional and elevation angles were within $3°$ and that in the pitch angle was within $4°$. In the present study, because the wing size of the phorid fly is much smaller than that of the hoverfly, the twist and camber deformations are smaller, and the errors can be smaller than the above values. It should be noted that when the left and right wings have asymmetric motions, as in the case of MSd, the Euler angles are different between the two wings, and thus the relative errors will be a little different between the two wings.

As mentioned earlier, we only found one phorid fly with natural wing area loss. Therefore, only this fly and another normal fly of the same size and weight are considered in the present work. The wing area loss is at the outer part of the wing: This part of the wing is important in aerodynamic force and moment generation, and our study can provide a good example of wing kinematic and aerodynamic compensations for wing damage in very small insects.

B. Aerodynamic force computation

We conducted a three-dimensional flow simulation to study the aerodynamics during the flapping flights of phorid flies.

The governing equations of the flows around the insects are the incompressible Navier-Stokes equations. Let us use c, U, and c/U as the reference length, speed, and time, respectively, to nondimensionalize the Navier-Stokes equations (c is the mean chord-length and U is defined as $U = 2\Phi f r_2$, where Φ is the stroke amplitude and is equal to the maximum stroke angle minus the minimum stroke angle, f is the wingbeat frequency, and r_2 is the radius of gyration of the wing). It is noted that the reference length and speed for the wing-damaged phorid fly are c and U of its intact wing. The nondimensionalized forms of the equations are

$$\nabla \cdot \mathbf{u} = \mathbf{0}, \tag{1}$$

$$\frac{\partial \mathbf{u}}{\partial \tau} + \mathbf{u} \cdot \nabla \mathbf{u} = -\nabla p + \left(\frac{1}{\text{Re}}\right)\nabla^2 \mathbf{u}, \tag{2}$$

where $\mathbf{u}$ is the nondimensional fluid velocity field, τ is the nondimensional time, p is the nondimensional fluid pressure, Re is the Reynolds number ($\text{Re} = cU/\nu$, where ν is the kinematic viscosity of the air; here, Re of the normal phorid fly is 40), and ∇ and ∇^2 are the gradient and Laplacian operators. The equations were numerically solved using a three-dimensional unsteady flow solver based on the method of artificial compressibility developed by Rogers *et al.* [23]. A detailed description of the flow solver can be found in previous studies of our group, and the validity of the flow solver has been well demonstrated [13,24,25]. As for the boundary conditions, at the far-field inflow boundary, the velocity components are specified according to the constant inflow velocity while pressure is extrapolated from the interior; at the far-field outflow boundary, pressure is set equal to the inflow pressure, and the velocity is extrapolated from the interior. On the wing surfaces, impermeable wall and no-slip boundary conditions are applied, and the pressure on the boundary is obtained through the normal component of the momentum equation.

Since the left and right wings were asymmetrical and had relative movements, moving overset grids were used in this study (Fig. 4). As was shown in previous studies, the effect of body-wing interaction on the aerodynamic force was negligibly small [26,27]. Therefore, only two wing models were considered. The thickness of each wing model is 3% of the local chord length. The thickness of the wing of a phorid fly is not known. In the literature on flow computation and flow measurement, some researchers used a value between 1% and 3% for the ratio between the model-wing thickness and the wing chord length (e.g., Refs. [24,26,28]), and many
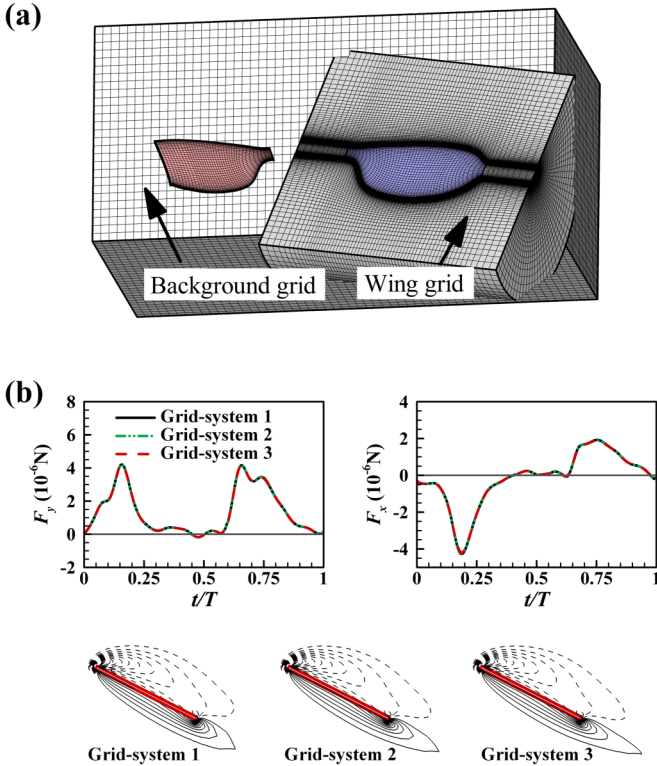
(a)

(b)

FIG. 4. (a) Portions of the computational grid system of the wing-damaged phorid fly. (b) Time courses of the force coefficients and contour plots of nondimensional spanwise component of vorticity at the span location r_2 for the right wing of the normal phorid fly (solid and broken lines indicate positive and negative vorticity, respectively; the magnitude of the nondimensional vorticity at the outer contour is 2, and the contour interval is 2), calculated with three grid systems.

researchers did not give this parameter in their paper (e.g., Refs. [29,30]). The reason for this may be that people believe that for low Re and separated flow on an insect's flapping wing, the flow is not very sensitive to the thickness of the wing. In a recent paper of our group [31], three thickness ratios (1%, 3%, and 5%) were considered in computations on a flapping wing, and the results showed that the forces computed by the three wing models are almost the same (differences in mean force coefficients are less than 2.5%). Therefore, we think that a 3% thickness ratio for the model wing of the phorid fly can be a reasonable choice.

Each of the wings had a body-fitted curvilinear grid of O-H type, and the background was a Cartesian grid that extended to the far-field boundary of the domain [Fig. 4(a)]. For the wing grids, dynamically deforming grids are used to treat the time-varying bending deformation. A procedure of combining the method of the modified *trans*-finite interpolation and the method of solving the Poisson equation was used to generate the dynamically deforming grids. A more detailed description of the procedure can be found in Ref. [32].

To ensure that the flow calculations were grid-independent, a grid resolution test was conducted using the wing models and wing kinematics of a normal phorid fly. Three grid systems were considered. For grid system 1, the wing grid had dimensions $43 \times 61 \times 43$ in the normal direction, around

the wing, and in the spanwise direction, respectively (the first-layer grid thickness was $0.0015c$); the background grid had dimensions $81 \times 81 \times 81$ in the X, Y, and Z directions, respectively. For grid system 2, the corresponding grid dimensions were $65 \times 91 \times 65$ and $121 \times 121 \times 121$ ($0.001c$). For grid system 3, the corresponding grid dimensions were $96 \times 135 \times 96$ and $181 \times 181 \times 181$ ($0.000\,67c$). For all three grid systems, the grid points of the wings were clustered densely toward the wing surface and toward the wake, and the grid points of the background grid were concentrated in the near field of the wings. The nondimensional time step was equal to $T/440$ (nondimensionalized by c/U). As shown in Fig. 4(b), there is almost no difference between the force coefficients calculated by the three grid systems; there is a small difference in the vorticity contour plots between grid system 2 and grid system 1, but almost no difference in vorticity contour plots between grid system 2 and grid system 3. This indicates that very good solution accuracy is achieved when grid system 2 or 3 is used. Here grid system 2 was used (for the damaged wing, due to the shorter wing length, fewer points were in the spanwise direction: the wing grid was changed to $65 \times 91 \times 59$).

III. RESULTS AND DISCUSSION

Based on our observations, we found that phorid flies do not perform hover flight and that they commonly perform low-speed forward flight. Therefore, this type of flight is focused on in this study. The phorid fly with natural damage on the left wing is denoted as MSd. The normal phorid fly used to compare with MSd is denoted as MSn. These two phorid flies playing low-speed forward flight with almost the same advance ratio J (the ratio between forward flight speed and average wingtip flapping speed) were filmed; their video sequences are shown in Fig. 5 (the original video sequences
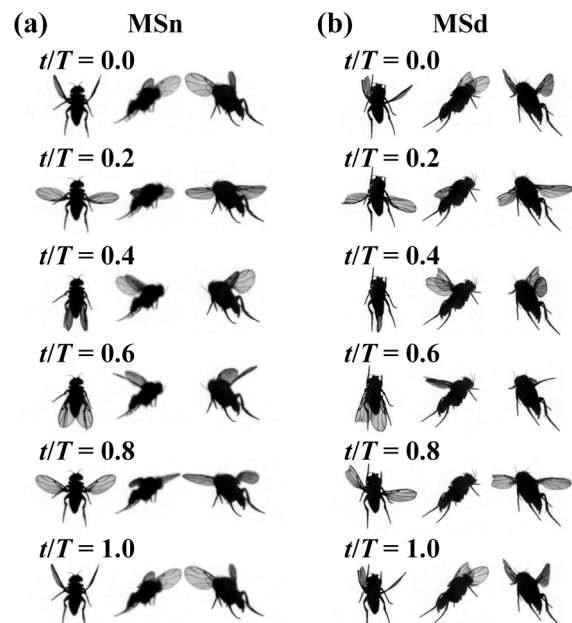

FIG. 5. Video sequences of MSn and MSd.

TABLE I. Morphological parameters.

ID	m (mg)	$R(R')$ (mm)	c (mm)	$S(S')$ (mm^2)	r_2/R	L_r (mm)	L_b (mm)	l (mm)	h (mm)
MSn	0.26	1.33	0.45	0.60	0.58	0.56	1.82	0.35	0.23
MSd	0.26	1.34 (1.07)	0.45	0.60 (0.50)	0.58	0.58	1.84	0.35	0.23

of MSn and MSd are presented as supplemental movie 1 and movie 2, respectively; see the Supplemental Material [33]).

A. Morphological parameters

The morphological parameters of the two phorid flies are given in Table I. Parameters in Table I include the total mass of an insect (m), wing length (R) (R' denotes the wing length of the damaged wing), mean chord-length of the wing (c), wing area (S) (S' denotes the wing area of the damaged wing), radius of gyration of the wing (r_2), distance between two wing roots (L_r), body length (L_b), distance between the wing-base axis and the center of mass (l), and distance between the wing-base axis and the body axis (h). It is seen that the morphological parameters of MSn and MSd are very similar, except that MSd has 16.7% wing area loss in the outer part of the left wing (Fig. 1). We use MSn to represent the undamaged status of MSd.

B. Wing kinematic compensation

Figure 6 shows the measured Euler angles and the maximum bending displacements of the wings of MSn and MSd. Based on the data in Fig. 6, stroke diagrams showing the flapping motions are plotted in Fig. 7, and the kinematic

parameters are given in Table II (in addition to the parameters mentioned above, χ, the angle between the body axis and the horizontal plane, and γ, the rolling angle of the body, are also included in the table).

As seen in Fig. 7, for the normal phorid fly, MSn, the two wings have approximately symmetric flapping modes: each wing has a U-shaped upstroke wing path and a relatively planar downstroke wing path [Fig. 7(a)], similar to the other very small insects studied in Refs. [13,14]. However, for the
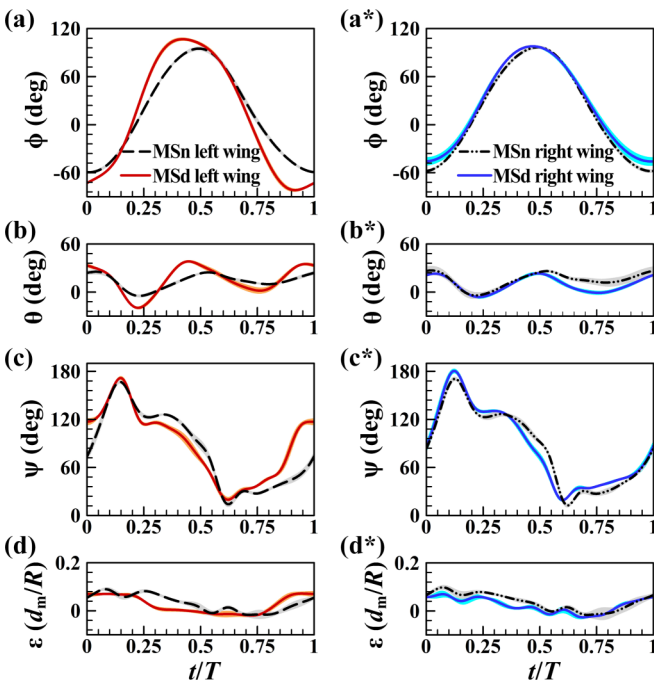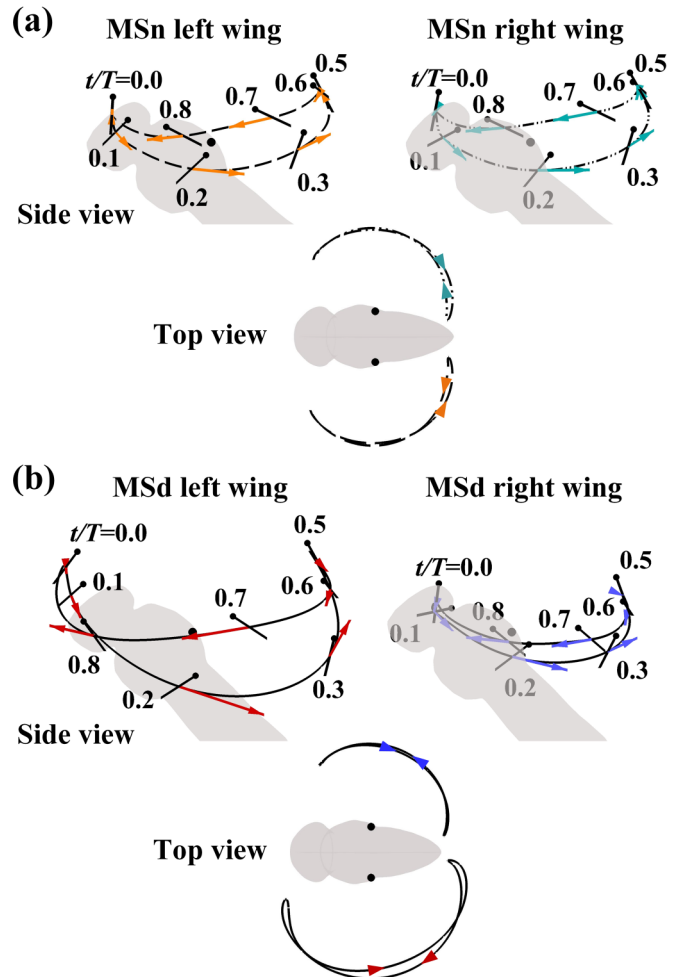

FIG. 7. Stroke diagrams show the wing motions of (a) MSn and (b) MSd. The curves indicate the wing paths at $0.58R$ from the wing roots; black dots on the bodies define the wing-root location; black lines in side view indicate the orientation of the wing at various times in one stroke cycle, with dots marking the leading edge; colored arrows in side view represent the velocities of the wing at $0.58R$ from the wing roots; colored arrows in top view indicate the flapping directions.

FIG. 6. Measured Euler angles and the maximum bending displacements of (a)–(d) the left wings and (a*)–(b*) right wings of MSn and MSd (mean $\pm$ s.d.; $n = 8$ wingbeats).

TABLE II. Kinematic parameters.

| ID | J | f (Hz) | Φ (deg) | | β (deg) | χ (deg) | γ (deg) |
			Left wing	Right wing			
MSn	0.23	332.17	154.44	154.69	6.79	37.24	0.20
MSd	0.20	308.54	188.58	143.87	0.61	42.43	0.10

phorid fly with the left wing damaged, MSd, to compensate for the wing area loss, the upstroke motion of the damaged left wing becomes more downward-curved compared to that of the intact left wing of MSn [Fig. 7(b)], giving a deeper U-shaped wing path. Moreover, the stroke amplitude Φ of the damaged left wing increases greatly, reaching the 180° limit. In addition to adjusting the kinematics of the damaged left wing, MSd also adjusts its intact right wing: it slightly decreases the stroke amplitude and increases the depth of the downstroke U-shaped wing path [Fig. 7(b)].

For the damaged wing of MSd, in the upstroke, the large Φ and the deep U-shaped wing path significantly increase the traveling distance, and thus increase the wing velocity (see the arrows in the side views of Fig. 7); in addition, in the beginning of the upstroke, the damaged wing accelerates downward with a large angle of attack (see the orientation of the wing section in the side views of Fig. 7). In the downstroke, the large Φ increases the wing velocity.

It is expected that the larger wing velocity during its flapping motion and the rapid downward acceleration with large angle of attack in the beginning of the upstroke will help the damaged wing generate the required aerodynamic force. The location of the total force of the damaged left wing will be different from the normal case, and hence its moment will be different from the normal case. Thus, it is expected that the kinematic adjustment of the intact right wing is associated with the balance of the moment. The problem of aerodynamic force generation and the balance of the forces and moments will be discussed in the next section.

Previous studies [5,6] indicated that medium and large insects, such as fruit flies and hawkmoths, compensate for unilateral wing damage mainly by increasing the stroke amplitude of the damaged wing, but here the results shows that for the very small insect phorid fly, in addition to the stroke amplitude, the deviation angle (or the depth of the U-shaped wing path) is also greatly increased for the compensation of the loss of the wing area.

C. Aerodynamic forces and moments

Using the kinematics measured above, the aerodynamic forces and moments acting on the phorid flies were computed using the flow solver described in Sec. II. For the phorid flies moving forward at $J \approx 0.2$ (Table II), the constant flight speed was given at the inflow boundary (see Sec. II), as was done in similar CFD studies on insect flight (e.g., Refs. [34,35]). As shown in Fig. 8, we use F_x, F_y, and F_z to denote the x, y, and z components of the aerodynamic force of a wing, respectively, and M_x, M_y, and M_z to denote the x, y, and z components of the moment of a wing about the center of mass, respectively.

In addition, we refer to the forces in the x, y, and z directions as vertical, horizontal, and side forces, respectively.

The time courses of F_x, F_y, and F_z for the wings of MSd are shown in Fig. 9. It is observed that the F_y (the vertical force) curves of the two wings of MSd are similar to each other, each of which has a large peak in the upstroke and a relatively lower peak in the downstroke [Fig. 9(a)]. The cycle-mean vertical forces of the damaged left wing and the intact right wing are almost the same, i.e., 1.32×10^{-6} and 1.35×10^{-6} N, respectively. The cycle-mean vertical force produced by the two wings is 2.67×10^{-6} N. Based on the data in Table I, the weight of the phorid fly is 2.55×10^{-6} N. The difference between vertical force and weight is less than 5%. We see that the vertical force produced can support the weight. As seen in Fig. 9(b), the F_x (the horizontal force) produced by the damaged left wing is larger than that produced by the intact right wing at the midportions of the upstroke and the downstroke, but in a whole stroke cycle, the large F_x of the damaged left wing in the upstroke cancels out F_x in the downstroke because they have opposite signs. As a result, the cycle-mean F_x of the damaged left wing is only 0.03×10^{-6} N, approximately zero. The upstroke and downstroke F_x of the intact right wing also cancel each other out, and the cycle-mean F_x of the intact right wing is only 0.06×10^{-6} N, also approximately zero. Thus, the cycle-mean horizontal force of the two wings is approximately zero. As seen in Fig. 9(c), in most of the
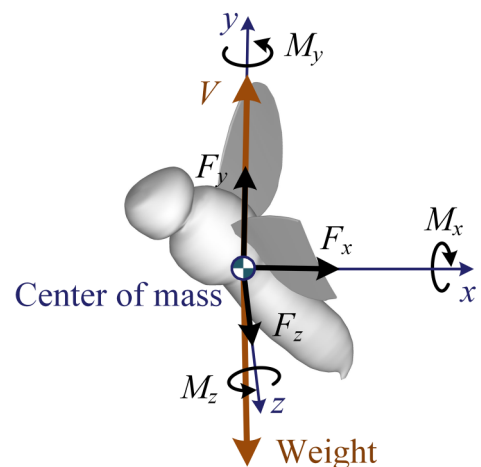

FIG. 8. Diagram used to define the forces and moments. F_x, F_y, and F_z denote the x, y, and z components of the aerodynamic force of a wing, respectively; M_x, M_y, and M_z denote the x, y, and z components of the moment of a wing about the center of mass, respectively; V is the total vertical force of the two wings. The direction of the axes in coordinate system (x, y, z) is the same as that in coordinate system (X, Y, Z).
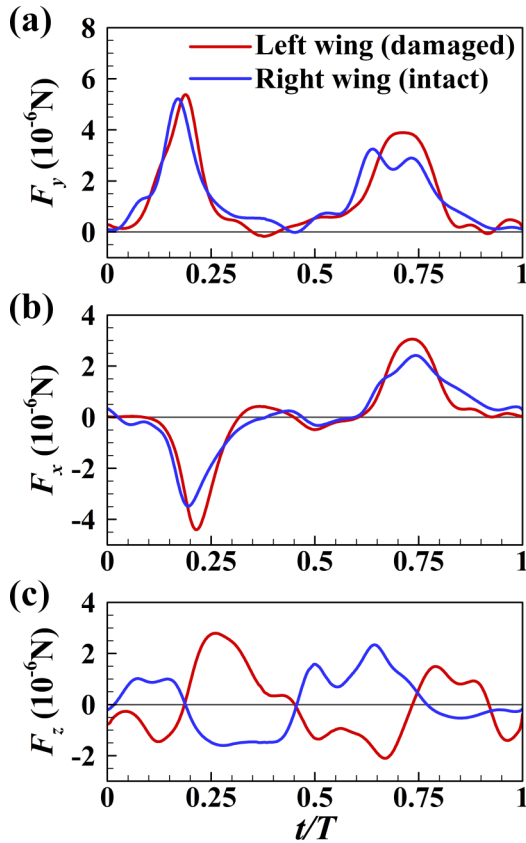
FIG. 9. Time courses of the computed forces (a) F_y, (b) F_x, and (c) F_z of the damaged left wing and the intact right wing of MSd.

FIG. 11. Contour of nondimensional spanwise component of vorticity of the two wings in the section at $0.58R$ from the wing roots. The vorticity is nondimensionalized by U/c; the counterclockwise and clockwise vorticity are denoted as solid and dashed lines, respectively; the magnitude of the nondimensional vorticity at the outer contour is 2, and the contour interval is 2.

stroke cycle, the magnitude of F_z of the damaged left wing is a little larger than that of the intact right wing, but it can be shown that the cycle mean side force of the two wings is 0.08×10^{-6} N, also approximately zero. We thus see that the force balance condition for steady flight is met with good accuracy.

As seen above, the damaged wing can produce the required vertical force after the kinematic adjustment. As mentioned earlier, this is expected to be associated with the larger wing velocity during the downstroke and upstroke and the rapid downward acceleration with a large angle of attack in the beginning of the upstroke. To see this more clearly, the time courses of the wing velocities at $0.58R$ from the wing roots are plotted in Fig. 10. It is seen that the maximum velocity
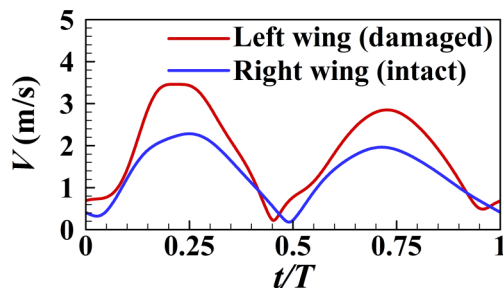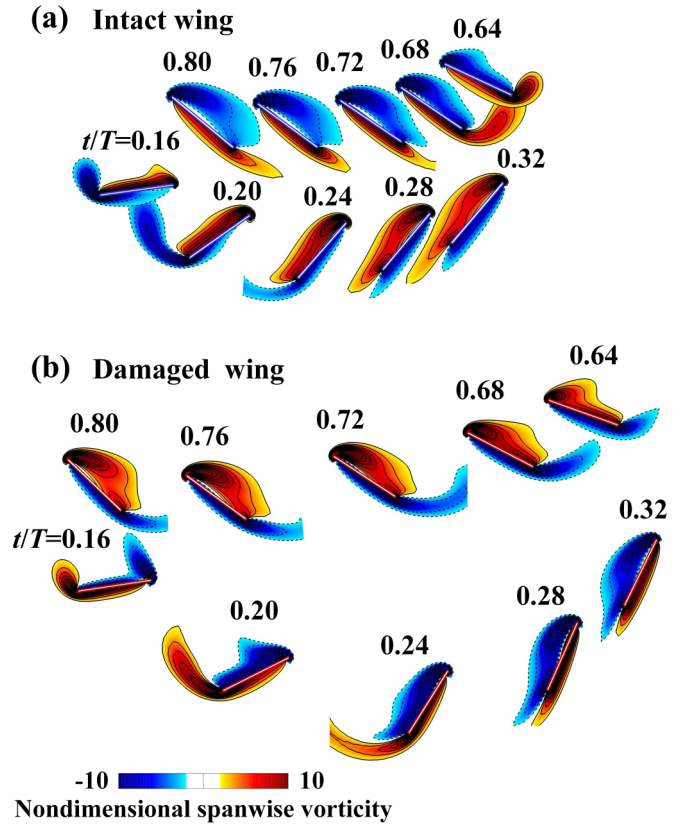
of the damaged wing is about 1.5 times that of the intact wing in both the upstroke and downstroke, and the slope of the velocity curve, i.e., the acceleration of the damaged wing at $t/T = 0.1 - 0.18$ (the beginning of the upstroke), is much larger than that of the intact wing. To explain the effect on the vertical force, vorticity fields are plotted for the period in which a large aerodynamic force is produced.

Figure 11 shows the vorticity contours of the two wings. During the midportions of the upstroke and downstroke, the leading-edge vortex (LEV) attaches and moves with the wing, indicating that the force production mechanism is the delayed-stall mechanism [24,28–30,36–40]. Figure 12 gives an overall picture of the vortical structure of the wings. For each wing, an attached LEV, a tip vortex and a root vortex leaving from the two ends of the wing, and a starting vortex in the wake form a "vortex ring." As the attached LEV moves forward with the wing, the "vortex ring" expands in size, giving the increased distance between the LEV and the starting vortex. From vorticity dynamics theory, the aerodynamic force on a body moving in an incompressible viscous flow is equal to the time rate of change in the first moment of vorticity [17,41,42]. Because the attached LEV and the starting vortex carry vorticities with opposite revolving directions, when the distance between the LEV and the starting vortex increases, a time rate of change in the first moment of vorticity will be

FIG. 10. Time courses of the wing velocities at $0.58R$ from the wing roots.
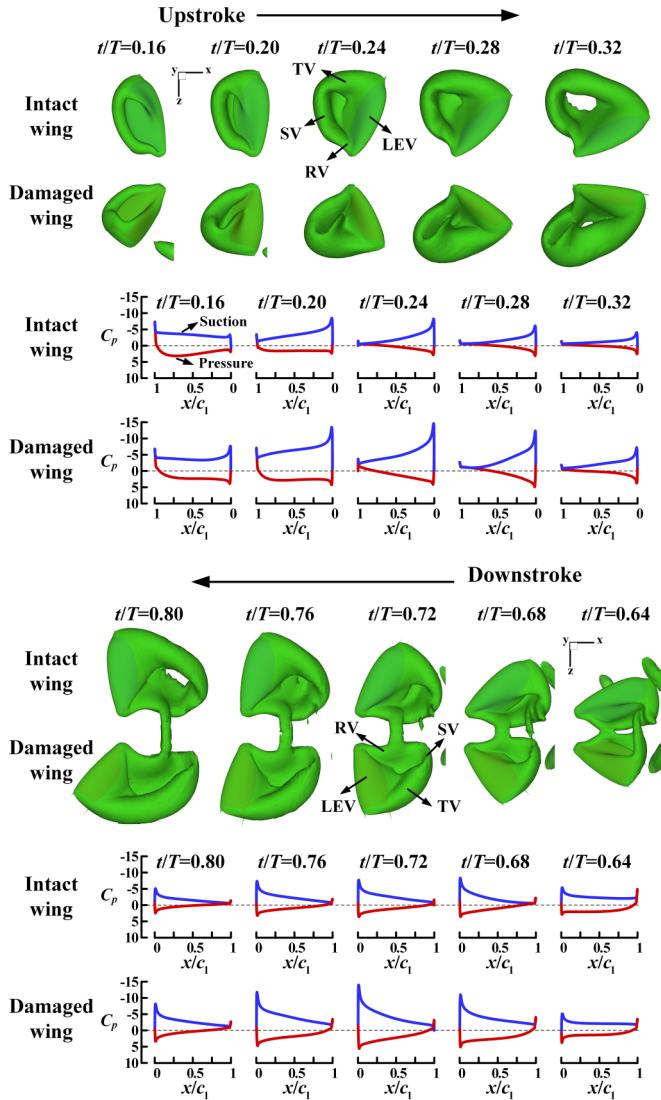
FIG. 12. Isovorticity surface plots and pressure distributions at section $0.58R$ for MSd during one stroke cycle. The vorticity is nondimensionalized by U/c and the magnitude of the nondimensional vorticity is 2. TV denotes tip vortex, RV denotes root vortex, and SV denotes starting vortex. The nondimensional pressure, C_P, is defined as $(p - p_\infty)/0.5\rho U^2$, where ρ is the fluid density.

FIG. 13. Time courses of the vertical component of the nondimensional total first moment of vorticity (γ_y), nondimensionalized by UcS, for the damaged left wing (a) and the intact right wing (b) of MSd, and the corresponding vertical forces (c) and (d).

generated. As shown in Fig. 12, although the "vortex ring" of the damaged wing is narrower in the spanwise direction, it expands faster in the direction of the motion, which increases the time rate of change in the first moment of vorticity, or the aerodynamic force of the damaged wing. To illustrate this point further, we computed and examined the time rate of change of the first moment of vorticity. Figures 13(a) and 13(b) show the time courses of the vertical component of the nondimensional total first moment of vorticity (γ_y) for the left and the right wings of MSd, respectively. The short lines on the γ_y-curve are the tangent lines of the curve, the slope of which represents the time rate of change of γ_y or the vertical force coefficient. During the periods of $t/T \approx 0.10-0.30$ and $t/T \approx 0.60-0.80$, the magnitude of γ_y of the wings continually increases, which is associated with the increased distance between the LEV and the starting vortex (Fig. 12). It
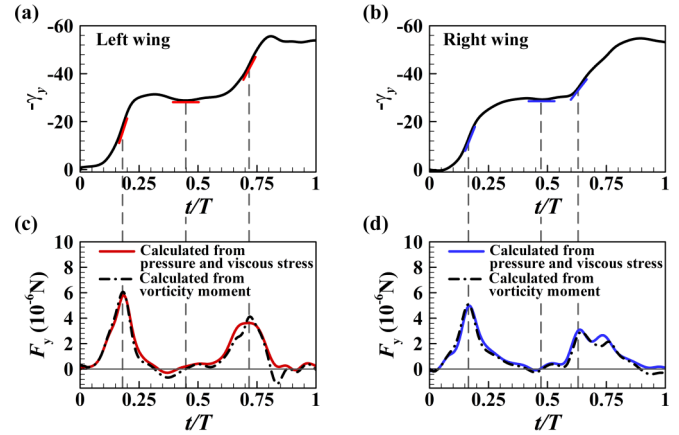
is seen that the slope of the γ_y-curve of the damaged left wing is similar to that of the intact right wing [see the slope of the short lines in Figs. 13(a) and 13(b)]. This indicates that the damaged left wing, which has a narrower "vortex ring" but a larger expanding velocity (Fig. 12), can generate the same time rate of change of the first moment of vorticity as the intact right wing, which has a wider "vortex ring" but a smaller expanding velocity (Fig. 12), explaining why the damaged left wing produces approximately the same vertical force as the intact right wing. The vertical forces calculated by taking the time derivative of the vorticity moment and those calculated in the usual way of integrating the pressure and viscous stress on the wing surface are plotted in Figs. 13(c) and 13(d) for the left and right wings, respectively (the result obtained from the time rate of change of the total first moment of vorticity and that obtained from the pressure and viscous stress on the wing surface are almost the same, as they should be). In the above computation of the vorticity moments, because of the asymmetrical left and right wings, separate flow simulations were done for each of the left and right wings. In addition, the results plotted in Fig. 13 are those of the first stroke cycle; this is because the vorticity in the wake after a few cycles will move far away from the wing, and the vorticity there is not accurate enough for the calculation (the grids are dispersive in the far field). Our computational results showed that for the forward flight of the very small phorid fly, the aerodynamic force of the first stroke cycle is approximately the same as that of the later stroke cycles; therefore, the results of the first stroke cycle are used here.

It is of interest to examine the pressure distributions on the surfaces of the intact and damaged wings. Figure 12 also includes the pressure distributions in the section at $0.58R$ from the wing roots. It is seen that during the midportions of the upstroke and downstroke, the attached LEV gives a large suction at the leading edge, and the force produced is dominated by the negative C_P on the upper surface of the wing. To produce the required aerodynamic force, the suction of the damaged wing at section $0.58R$ is much larger than that of the intact wing. This is expected because the wing velocity
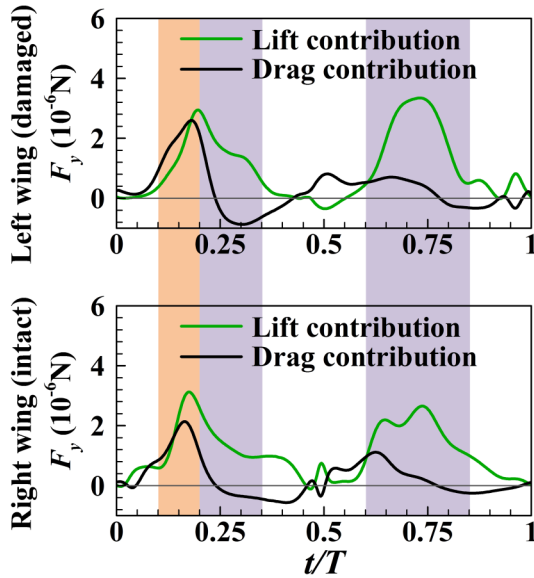
FIG. 14. Contributions of lift and drag to the vertical force of the left and right wings of MSd in one stroke cycle. The orange background indicates where the drag has a larger contribution to the vertical force for the damaged wing, and purple indicates where the lift has a larger contribution.

of the damaged wing is much larger than that of the intact wing.

To investigate the effect of large downward acceleration with a large angle of attack in the beginning of the upstroke, the contributions of lift and drag of the wings to the vertical force are plotted in Fig. 14, where the lift and drag are the two components of the total aerodynamic force, which are perpendicular and parallel to the wing velocity, respectively. It is seen that during most periods, lift makes more of a contribution to the vertical force for both wings, but in the beginning of the upstroke, the drag of the damaged wing makes more of a contribution to its vertical force. This indicates that in the beginning of the upstroke, the damaged wing generates more upward drag through accelerating downward with a large angle of attack, which makes a large contribution to the weight-supporting vertical force. The effect of the large downward acceleration can also be seen from the pressure distributions in Fig. 12. At $t/T = 0.16$ and 0.20 (Fig. 12), a significant part of the force of the damaged wing comes from the positive C_P on the lower surface of the wing. As the wing accelerates downward, it smashes on the air, producing pressure on the lower surface. This helps the damaged wing produce more aerodynamic force.

The damaged wing can produce the required vertical force via the increased wing velocity in the upstroke and down-stroke and the large wing acceleration in the beginning of the upstroke. As mentioned earlier, the large wing velocity and the large acceleration of the damaged wing come from the increased stroke amplitude and deviation angle. It is of interest to see the respective effect of the stroke amplitude and the deviation angle on the force production. For this purpose, we conducted two additional computations: In one case, the stroke amplitude of the damaged wing was decreased to that of the normal wing of MSn; in the other case, the amplitude of
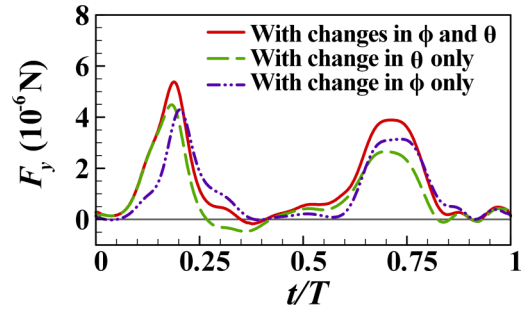

FIG. 15. Respective effect of changes in the deviation and the stroke amplitude on the vertical force of the damaged wing.

the deviation angle of the damaged wing was decreased to that of the normal wing of MSn. The results are shown in Fig. 15. It is seen that both of the compensational changes in ϕ and θ are very important for the force production. In the beginning of the upstroke ($t/T \approx 0-0.17$), the change in ϕ has little effect on F_y, while the change in θ significantly decreases F_y, indicating that the vertical force produced in the beginning of the upstroke is mainly affected by the change in θ. This is expected because the deep U-shaped wing path is produced by the large deviation angle, which gives the damaged wing a large downward acceleration. In the rest of the stroke cycle ($t/T \approx 0.17-1$), the vertical force is affected by the changes in both ϕ and θ, because both changes affect the wing velocity. But it should be noted (Fig. 15) that in the midportion of the downstroke ($t/T \approx 0.65-0.85$), the change in ϕ has a larger effect on F_y than the change in θ.

In the above, we have discussed the aerodynamic forces and force balance. If an insect wants to maintain a stable flight, not only does weight-supporting vertical force need to be produced, but also the moment about the center of mass should be zero. The time courses of M_x, M_y, and M_z for each of the wings are given in Fig. 15.

As shown in Fig. 16, the magnitude of M_x of the damaged left wing is approximately the same as that of the intact right wing, but their signs are opposite, thus the M_x of the two wings can cancel each other out. This is also true for M_y. The M_z's of the two wings have both similar magnitudes and signs, but they change their signs at the middle of the upstroke and the downstroke, which can cancel themselves out in one stroke cycle. Based on the data in Fig. 16, the cycle-mean moments of each wing of MSd are calculated (Table III), $M_{x,m}$, $M_{y,m}$, and $M_{z,m}$ denoting the mean values of M_x, M_y, and M_z, respectively. Adding up the data of the two wings in Table III, the moments of the wing-damaged phorid fly about the x-axis, y-axis, and z-axis are all close to zero, namely 0.08×10^{-9}, -0.07×10^{-9}, and 0.01×10^{-9} N m, respectively. This indicates that the zero-moment condition for stable flight is also met with good accuracy. It is noted that if a normal insect flies in a balanced condition, due to the symmetrical kinematics of the two wings, the M_z of each wing needs to cancel itself out in one stroke cycle. But for a damaged phorid fly, after kinematic adjustments, the magnitude of the M_z of the damaged left wing is larger than that of the balanced condition, which needs to be balanced by the intact right wing. This explains why the intact wing also needs to adjust the wing kinematics.
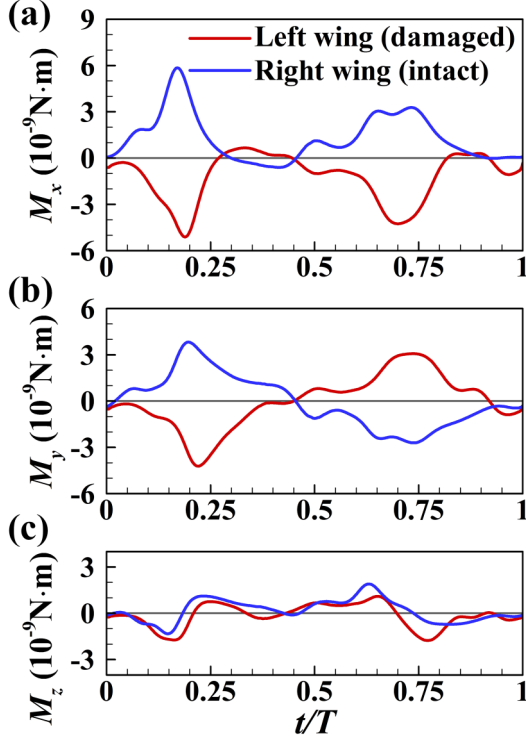
FIG. 16. Time courses of the computed moments (a) M_x, (b) M_y, and (c) M_z of the damaged left wing and the intact right wing of MSd.

The above results show that the damaged wing of the small phorid fly can produce the required vertical force through using a larger wing velocity during its flapping motion and a rapid downward acceleration at a large angle of attack in the beginning of the upstroke. However, to compensate for the area loss in the left wing, the stroke amplitude of the damaged left wing has already reached the 180° limit, and the U-shaped upstroke wing path is very deep, also approaching its limit. That is, although the wing-damaged phorid fly can now achieve a stable flight, there is not much room for the fly to further adjust its wing kinematics for maneuvers, which may affect the performance of escape, predation, competition, etc. The mortality possibility of the wing-damaged phorid fly is greatly increased.

Furthermore, as discussed above, the magnitude of the instantaneous vertical force (F_y) of the damaged left wing is approximately equal to that of the intact right wing, while the magnitudes of the instantaneous horizontal (F_x) and side (F_z) forces of the damaged left wing are larger than their counterparts of the intact right wing. Thus, it is expected that the damaged wing endures larger aerodynamic force than that in the normal case. To see this, we compare the resultant aerodynamic force (denoted as F) of the wing-damaged phorid

TABLE III. Aerodynamic moments.

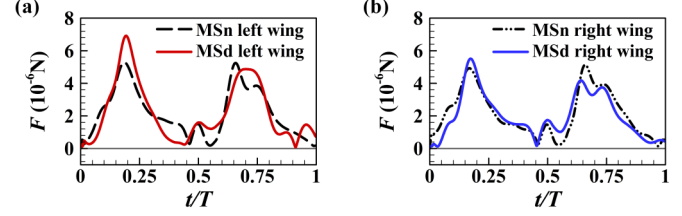| ID		$M_{x,m}$ (μN mm)	$M_{y,m}$ (μN mm)	$M_{z,m}$ (μN mm)
MSd	Left wing (damaged)	−1.22	−0.02	−0.16
	Right wing (intact)	1.30	−0.05	0.17

FIG. 17. Time courses of the resultant aerodynamic force of (a) the left wings and (b) the right wings of MSn and MSd.

fly (MSd) with that of the normal phorid fly (MSn). F is computed as

$$F = \sqrt{F_x{}^2 + F_y{}^2 + F_z{}^2}. \qquad (3)$$

Figure 17 shows the time course of the resultant aerodynamic force for each wing of MSn and MSd. It is seen that the peak value in the force-curve of the damaged left wing of MSd is 31% larger than that of the corresponding wing of MSn (the cycle-mean aerodynamic force produced by the damaged left wing of MSd is 4.5% larger than that of the corresponding wing of MSn). Due to the larger aerodynamic force and the smaller wing area, the cycle-mean wing loading (cycle-mean aerodynamic force divided by wing area) of the damaged left wing of MSd is 25% larger than that of the corresponding wing of MSn (the cycle-mean wing loading of the damaged left wing of MSd is 4.5 N/m^2, but that of the left wing of MSn is only 3.6 N/m^2). The very large wing loading on the damaged wing may greatly shorten the life of the damaged wing.

D. Power consumption

The energy expenditure is a crucial parameter to quantify the flight performance of the wing-damaged insect. As mentioned earlier, previous studies measured the metabolic costs (oxygen consumption rates or CO_2 production rates) to estimate the energy expenditures of the wing-damaged insects [2,9], but it is not known how the insects distribute the energy to the damaged wing and the normal wing. Here, to investigate the energy distribution between the damaged and intact wings, we computed the power consumption of each wing of the normal phorid fly (MSn) and the wing-damaged phorid fly (MSd), based on the aerodynamic force and the kinematic data above. The mechanical power (P) of a flapping wing consists of two parts, namely the aerodynamic power (P_a) and the inertial power (P_i). P_a is produced by the wing-stroke muscles to overcome the aerodynamic moment ($\boldsymbol{M_a}$), and it can be calculated by

$$P_a = \boldsymbol{M_a} \cdot \boldsymbol{\Omega}, \qquad (4)$$

where $\boldsymbol{\Omega}$ is the angular velocity of the wing. The inertial power is produced by the wing-stroke muscles to overcome the inertial moment ($\boldsymbol{M_i}$), and it can be calculated by

$$P_i = \boldsymbol{M_i} \cdot \boldsymbol{\Omega}. \qquad (5)$$

The aerodynamic power P_a can be calculated readily as $\boldsymbol{M_a}$ and $\boldsymbol{\Omega}$ of each wing are known. However, the calculation of the inertial power P_i is not so straightforward, because
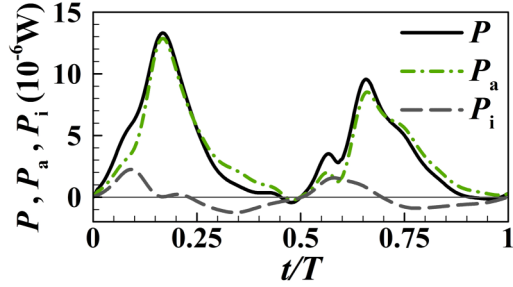
FIG. 18. Time courses of the mechanical power P, aerodynamic power P_a, and inertial power P_i of the right wing of MSn.

the mass (m_w) and the radius of gyration ($r_{2,m}$) of the wing required for computing M_i are unknown for phorid flies.

We deal with this problem in the following way. The wing-to-body mass ratio (m_w/m) and the nondimensional radius of gyration ($r_{2,m}/R$) for a larger fly species, *Drosophila virilis*, are known [43]: $m_w/m = 0.24\%$ and $r_{2,m}/R = 0.48$. It has been found that $r_{2,m}/R$ in dipterans typically lies at 0.4–0.5R [19] and that the wing-to-body mass ratio (m_w/m) tends to decreases as the wing size decreases: wing mass is mostly contributed by the wing veins [18], and the number of wing veins is reduced as the wing size decreases [44,45]. As a result, if we take the values of m_w/m and $r_{2,m}/R$ of the fruit fly as those of our phorid flies, an overestimated M_i for the phorid flies is obtained. Figure 18 plots the time courses of P, P_a, and P_i of the right wing of MSn calculated using such an overestimated M_i. As seen in the figure, even if the inertial moment is overestimated here, the contribution of P_i is much smaller than P_a, and the curve of P is approximately the same as that of P_a; moreover, the difference between P and P_a, caused by P_i, is positive in the first half of an upstroke ($t/T \approx$ 0–0.25) or downstroke ($t/T \approx 0.5$–0.75 and is negative in the next half of an upstroke ($t/T \approx 0.25$–0.5) or downstroke ($t/T \approx 0.75$–1). This indicates that for the small insect, the effect of inertial power on the power consumption (the cycle-mean mechanical power) is very small. Commonly, when researchers consider power consumption, they compute two limiting cases and the real power consumption lies between the values of the two limiting cases [46,47]. One limiting case is 100% elastic energy storage (the negative inertial work can be completely stored in an elastic element and later released to do positive work). In this case, the cycle-mean mechanical power (P_m) simply equals the cycle-mean aerodynamic power ($P_{a,m}$). The other limiting case is 0% elastic energy storage (no negative inertial power can be stored for later use). Using the data in Fig. 18, the cycle-mean mechanical power in the case of 100% elastic energy storage is 3.50×10^{-6} W and that in the case of 0% elastic energy storage is 3.52×10^{-6} W; the difference is less than 1%. Since the two limiting values are approximately the same, any one of the limiting cases is a good approximation of the real case. Here we adopt the case of 100% elastic energy storage, computing the power consumption only by aerodynamic power (positive inertial power and negative inertial power cancel out). That is, in the following, we take the aerodynamic power as the total power consumption of the wing.
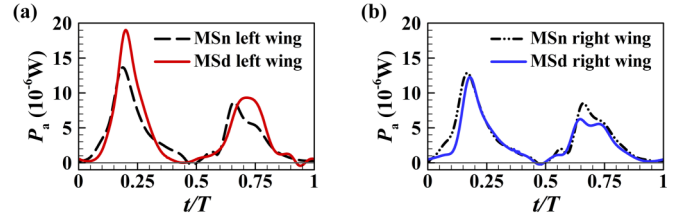

FIG. 19. Time courses of the aerodynamic power of (a) the left wings and (b) the right wings of MSn and MSd.

The time histories of the computed aerodynamic power for each wing of MSn and MSd are shown in Fig. 19. $P_{a,m}$ of each wing and the mass-specific power (P^*), which is defined as the total $P_{a,m}$ of an insect divided by the mass of the insect, are given in Table IV.

From the data in Table IV, it is seen that the normal phorid fly (MSn) and the wing-damaged phorid fly (MSd) have almost the same power expenditure, 7.09×10^{-6} and 7.05×10^{-6} W, respectively; because MSd and MSn have same mass on weight, their mass-specific power is approximately the same. That is, the flight of the wing-damaged phorid fly does not consume more power than that of a normal phorid fly. This conclusion is similar to that obtained for bumblebees with symmetric wing damage, using the method of measuring the metabolic costs (measuring the CO_2 production rate) [2]. When the metabolic-costs approach is used, the total energy consumed by the two wings can be obtained, but it is not known how the energy is distributed to each of the wings. With our computational approach, energy consumed by each of the wings can be readily calculated. The results are given in Table IV. As can be seen from the table, the distribution of the aerodynamic power between the damaged wing and the intact wing is highly asymmetrical: the aerodynamic power consumed by the damaged wing of MSd is 4.09×10^{-6} W, which is 38% larger than that by the intact wing of MSd (2.96×10^{-6} W).

Let us look at how the highly asymmetrical aerodynamic power occurs. As seen from Eq. (4), the power is the inner product of the aerodynamic moment and the angular velocity, i.e., it depends on the magnitude of $\boldsymbol{\Omega}$ and the component of M_a in the direction of $\boldsymbol{\Omega}$. From the data in Sec. III B, it is seen that the damaged left wing has a larger $\boldsymbol{\Omega}$ than the intact right wing. The component of M_a in the direction of $\boldsymbol{\Omega}$, denoted as M_P ($M_P = M_a \cdot \boldsymbol{\Omega}/|\boldsymbol{\Omega}|$), for each of the two wings of MSd is plotted in Fig. 20. It is seen that in the midportions of the upstroke and the downstroke, where the angular velocity of the damaged wing is very large, the M_P of the damaged wing is also larger than that of the intact wing. This explains why the aerodynamic power consumed by the damaged wing is

TABLE IV. Aerodynamic power.

| ID | $P_{a,m}$ (10^{-6} W) | | P^* (W/kg) |
	Left wing	Right wing	
MSn	3.59	3.50	27.27
MSd	4.09	2.96	27.12
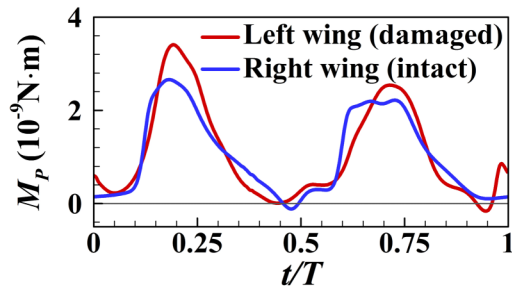
FIG. 20. Time course of M_P, the component of $\boldsymbol{M}_\mathbf{a}$ in the direction of $\boldsymbol{\Omega}$, of the damaged left wing compared with that of the intact right wing.

far more than that consumed by the intact wing. The fact that the phorid fly with a damaged wing needs to provide highly asymmetrical energy may greatly increase the muscle wastage of the damaged side.

A point is noted from the above results: Each wing of the normal phorid fly (MSn) consumes about 3.5 μW power (Table IV), while the intact wing of the wing-damaged phorid fly (MSd) consumes less power, about 3.0 μW (Table IV). This is a bit counterintuitive; if the wing kinematics used by the intact wing of MSd is more efficient, why does MSn not use this wing kinematics instead of the natural wing kinematics? A possible explanation is as follows: MSn is in a balanced level forward flight with natural wing kinematics. When other wing kinematics is used, the forces and moments will not be in balance.

IV. CONCLUSION

To compensate for the unilateral wing damage (16.7% wing area loss in the outer part of the left wing), the very small insect phorid fly (*Megaselia scalaris*) greatly increases the stroke amplitude and the deviation angle of the damaged wing (the large deviation angle gives the wing a deep U-shaped wing path), unlike the medium and large insects studied previously, which compensate for unilateral wing damage mainly by increasing the stroke amplitude of the damaged wing. The increased stroke amplitude and the deep U-shaped wing path give the damaged wing a larger wing velocity during its flapping motion, and in addition, the deep U-shaped wing path gives the damaged wing a rapid downward acceleration in the beginning of the upstroke. These enable the damaged wing to generate the required vertical force for weight support. However, the larger wing velocity of the damaged wing also generates larger horizontal and side forces. Although the larger horizontal and side forces of the damaged wing do not affect the force balance because these forces cancel themselves out in the stroke cycle, they increase the resultant aerodynamic force on the damaged wing. Due to the larger aerodynamic force and the smaller wing area, the wing loading of the damaged wing is 25% larger than that of the wings of the normal phorid fly, which may greatly shorten the life of the damaged wing. Furthermore, because the damaged wing has a much larger angular velocity and produces a larger aerodynamic moment compared with the intact wing of the damaged phorid fly, the aerodynamic power consumed by the damaged wing is 38% larger than that consumed by the intact wing, i.e., the energy distribution between the damaged wing and the intact wing is highly asymmetrical, which may greatly increase the muscle wastage of the damaged side.

[1] R. V. Cartar, Morphological senescence and longevity: An experiment relating wing wear and life span in foraging wild bumble bees, J. Anim. Ecol. **61**, 225 (1992).

[2] A. Hedenström, C. P. Ellington, and T. J. Wolf, Wing wear, aerodynamics and flight energetics in bumblebees (*Bombus terrestris*): An experimental study, Funct. Ecol. **15**, 417 (2001).

[3] S. A. Combes, J. D. Crall, and S. Mukherjee, Dynamics of animal movement in an ecological context: Dragonfly wing damage reduces flight performance and predation success, Biol. Lett. **6**, 426 (2010).

[4] B. Jantzen and T. Eisner, Hindwings are unnecessary for flight but essential for execution of normal evasive flight in Lepidoptera, Proc. Natl. Acad. Sci. USA **105**, 16636 (2008).

[5] M. J. Fernandez, D. Springthorpe, and T. L. Hedrick, Neuromuscular and biomechanical compensation for wing asymmetry in insect hovering flight, J. Exp. Biol. **215**, 3631 (2012).

[6] F. T. Muijres, N. A. Iwasaki, M. J. Elzinga, J. M. Melis, and M. H. Dickinson, Flies compensate for unilateral wing damage through modular adjustments of wing and body kinematics, Interface Focus **7**, 20160103 (2017).

[7] Z. Kassner, E. Dafni, and G. Ribak, Kinematic compensation for wing loss in flying damselflies, J. Insect Physiol. **85**, 1 (2016).

[8] C. A. Haas and R. V. Cartar, Robust flight performance of bumble bees with artificially induced wing wear, Can. J. Zool. **86**, 668 (2008).

[9] M. J. Fernández, M. E. Driver, and T. L. Hedrick, Asymmetry costs: Effects of wing damage on hovering flight performance in the hawkmoth *Manduca sexta*, J. Exp. Biol. **220**, 3649 (2017).

[10] K. N. Weaver, S. E. Alfano, A. R. Kronquist, and D. M. Reeder, Healing rates of wing punch wounds in free-ranging little brown myotis (*Myotis lucifugus*), Acta Chiropterol. **11**, 220 (2009).

[11] P. Chai, Hummingbird hovering energetics during moult of primary flight feathers, J. Exp. Biol. **200**, 1527 (1997).

[12] C. Shen, Y. Liu, and M. Sun, Lift and power in fruitflies in vertically-ascending flight, Bioinspir. Biomim. **13**, 056008 (2018).

[13] X. Cheng and M. Sun, Very small insects use novel wing flapping and drag principle to generate the weight-supporting vertical force, J. Fluid Mech. **855**, 646 (2018).

[14] Y. Z. Lyu, H. J. Zhu, and M. Sun, Flapping-mode changes and aerodynamic mechanisms in miniature insects, Phys. Rev. E **99**, 012419 (2019).

[15] J. H. Wu and M. Sun, Unsteady aerodynamic forces of a flapping wing, J. Exp. Biol. **207**, 1137 (2004).

[16] L. A. Miller and C. S. Peskin, When vortices stick: An aerodynamic transition in tiny insect flight, J. Exp. Biol. **207**, 3073 (2004).

[17] Y. Z. Lyu, H. J. Zhu, and M. Sun, Aerodynamic forces and vortical structures of a flapping wing at very low Reynolds numbers, Phys. Fluids **31**, 041901 (2019).

[18] R. Dudley, *The Biomechanics of Insect Flight: Form, Function, Evolution* (Princeton University Press, Princeton, NJ, 2002).

[19] C. P. Ellington, The aerodynamics of hovering insect flight. II. Morphological parameters, Philos. Trans. R. Soc. London, Ser. B **305**, 17 (1984).

[20] S. N. Fry, R. Sayaman, and M. H. Dickinson, The aerodynamics of free-flight maneuvers in Drosophila, Science **300**, 495 (2003).

[21] Y. P. Liu and M. Sun, Wing kinematics measurement and aerodynamics of hovering droneflies, J. Exp. Biol. **211**, 2014 (2008).

[22] X. L. Mou, Y. P. Liu, and M. Sun, Wing motion measurement and aerodynamics of hovering true hoverflies, J. Exp. Biol. **214**, 2832 (2011).

[23] S. E. Rogers, D. Kwak, and C. Kiris, Steady and unsteady solutions of the incompressible Navier-Stokes equations, AIAA J. **29**, 603 (1991).

[24] M. Sun and J. Tang, Unsteady aerodynamic force generation by a model fruit fly wing in flapping motion, J. Exp. Biol. **205**, 55 (2002).

[25] M. Sun and X. Yu, Aerodynamic force generation in hovering flight in a tiny insect, AIAA J. **44**, 1532 (2006).

[26] H. Aono, F. Liang, and H. Liu, Near- and far-field aerodynamics in insect hovering flight: An integrated computational study, J. Exp. Biol. **211**, 239 (2008).

[27] X. Yu and M. Sun, A computational study of the wing-wing and wing-body interactions of a model insect, Acta Mech. Sin. **25**, 421 (2009).

[28] C. P. Ellington, C. V. D. Berg, A. P. Willmott, and A. L. R. Thomas, Leading-edge vortices in insect flight, Nature (London) **384**, 626 (1996).

[29] H. Liu, C. P. Ellington, K. Kawachi, C. V. D. Berg, and A. P. Willmott, A computational fluid dynamic study of hawkmoth hovering, J. Exp. Biol. **201**, 461 (1998).

[30] G. Liu, H. Dong, and C. Li, Vortex dynamics and new lift enhancement mechanism of wing-body interaction in insect forward flight, J. Fluid Mech. **795**, 634 (2016).

[31] L. G. Liu and M. Sun, Dynamic flight stability of hovering mosquitoes, J. Theor. Biol. **464**, 149 (2019).

[32] G. Du and M. Sun, Effects of unsteady deformation of flapping wing on its aerodynamic forces, Appl. Math. Mech.–Engl. Ed. **29**, 731 (2008).

[33] See Supplemental Material at http://link.aps.org/supplemental/10.1103/PhysRevE.101.012412 for the movies of the two insects.

[34] C. Li, H. Dong, and K. Zhao, A balance between aerodynamic and olfactory performance during flight in Drosophila, Nat. Commun. **9**, 3215 (2018).

[35] T. Engels, D. Kolomenskiy, K. Schneider, F. O. Lehmann, and J. Sesterhenn, Bumblebee Flight in Heavy Turbulence, Phys. Rev. Lett. **116**, 028103 (2016).

[36] M. H. Dickinson, F. O. Lehmann, and S. P. Sane, Wing rotation and the aerodynamic basis of insect flight, Science **284**, 1954 (1999).

[37] R. J. Bomphrey, R. B. Srygley, G. K. Taylor, and A. L. R. Thomas, Visualizing the flow around insect wings, Phys. Fluids **14**, S4 (2002).

[38] S. P. Sane, The aerodynamics of insect flight, J. Exp. Biol. **206**, 4191 (2003).

[39] Z. J. Wang, Dissecting insect flight, Annu. Rev. Fluid Mech. **37**, 183 (2005).

[40] D. D. Chin and D. Lentink, Flapping wing aerodynamics: From insects to vertebrates, J. Exp. Biol. **219**, 920 (2016).

[41] J. C. Wu, Theory for aerodynamic force and moment in viscous flows, AIAA J. **19**, 432 (1981).

[42] H. J. Zhu and M. Sun, Unsteady aerodynamic force mechanisms of a hoverfly hovering with a short stroke-amplitude, Phys. Fluids **29**, 081901 (2017).

[43] S. Vogel, Flight in Drosophila: I. Flight performance of tethered flies, J. Exp. Biol. **44**, 567 (1966).

[44] A. A. Polilov, Small is beautiful: Features of the smallest insects and limits to miniaturization, Annu. Rev. Entomol. **60**, 103 (2015).

[45] D. L. Grodnitsky, *Form and Function of Insect Wings* (The Johns Hopkins University Press, Baltimore, 1999).

[46] T. Weis-Fogh, Energetics of hovering flight in hummingbirds and in Drosophila, J. Exp. Biol. **56**, 79 (1972).

[47] C. P. Ellington, The aerodynamics of hovering insect flight. VI. Lift and power requirements, Philos. Trans. R. Soc. London, Ser. B **305**, 145 (1984).